Highlights

An in-silico assessment of efficacy of two novel intra-cardiac electrode configurations versus traditional anti-tachycardia pacing therapy for terminating sustained ventricular tachycardia

Shuang Qian,Adam Connolly,Caroline Mendonca-Costa,Fernando Campos,Steven E. Williams,John Whitaker,Christopher A. Rinaldi,Martin J. Bishop

- Low-energy electrotherapy protocols suggest promise of reducing strong shocks

- Our 2 novel electrode configurations specifically target the arrhythmic substrate

- Their efficacies on terminating sustained VTs are higher than ATP

- Our 'transmural' configuration requires<1J shock energy

An in-silico assessment of efficacy of two novel intra-cardiac electrode configurations versus traditional anti-tachycardia pacing therapy for terminating sustained ventricular tachycardia

Shuang Qian[a],[*],[1], Adam Connolly[b], Caroline Mendonca-Costa[a], Fernando Campos[a], Steven E. Williams[a], John Whitaker[a,c], Christopher A. Rinaldi[a,c] and Martin J. Bishop[a]

[a]*School of Biomedical Engineering and Imaging Sciences, Rayne Institute, King's college London, 4th Floor, Lambeth Wing, St. Thomas' Hospital, Westminster Bridge Road, London,United Kingdom, SE1 7EH*

[b]*Invicro, Burlington Danes Building, Du Cane Rd, London,United Kingdom, W12 0NN*

[c]*Department of Cardiology, Guy's and St Thomas' Hospital, London,United Kingdom, SE1 7EH*

ABSTRACT

The implanted cardioverter defibrillator (ICD) is an effective direct therapy for the treatment of cardiac arrhythmias, including ventricular tachycardia (VT). Anti-tachycardia pacing (ATP) is often applied by the ICD as the first mode of therapy, but is often found to be ineffective, particularly for fast VTs. In such cases, strong, painful and damaging backup defibrillation shocks are applied by the device. Here, we propose two novel electrode configurations: "bipolar" and "transmural" which both combine the concept of targeted shock delivery with the advantage of reduced energy required for VT termination. We perform an in silico study to evaluate the efficacy of VT termination by applying one single (low-energy) monophasic shock from each novel configuration, comparing with conventional ATP therapy. Both bipolar and transmural configurations are able to achieve a higher efficacy (93% and 85%) than ATP (45%), with energy delivered similar to and two orders of magnitudes smaller than conventional ICD defibrillation shocks, respectively. Specifically, the transmural configuration (which applies the shock vector directly across the scar substrate sustaining the VT) is most efficient, requiring typically less than 1 J shock energy to achieve a high efficacy. The efficacy of both bipolar and transmural configurations are higher when applied to slow VTs (100% and 97%) compared to fast VTs (57% and 29%). Both novel electrode configurations introduced are able to improve electrotherapy efficacy while reducing the overall number of required therapies and need for strong backup shocks.

1. Introduction

Ventricular tachycardia (VT) is an important cause of mortality and morbidity. Patients with previous VT or at risk of VT may receive an implanted cardioverter defibrillator (ICD), which automatically detects and delivers appropriate electrotherapy to terminate the VT. Although ICDs decrease the risk of sudden cardiac death (SCD) and improve mortality [1], many significant clinical challenges remain. Strong defibrillation shocks are delivered from ICDs to terminate episodes of (otherwise lethal) ventricular fibrillation (VF), as well as fast and polymorphic VTs. Such strong shocks are extremely painful and can cause long-term damage to cardiac tissue in patients receiving frequent therapies, which reduces patient quality of life (QOL) [2, 3] and is associated with increased mortality [4]. Current ICDs often initially deploy anti-tachycardia pacing (ATP) in order to attempt to terminate the VT, keeping the strong defibrillation shock as backup. ATP involves the delivery of several sequences of pacing stimulus at a slightly higher rate than the VT, in order that the paced stimulus may interact with the centre of reentrant circuit to eliminate the excitable gaps that help to sustain the VT. Although ATP is found to be effective at terminating slow VTs (VT cycle length (Cl) >320 ms), it is

less efficacious in fast VTs (VTCl between 240 ms and 320 ms), reported to be as low as 50-79% [5, 6, 7].

In addition to stimulation through an electrode directly in contact with the heart (like in ATP), cardiac tissue can also be activated by "virtual electrodes (VE)"; whereby extracellular electrodes remote from the heart cause the existence of regions of hyperpolarisation or depolarisation within the myocardium. VE formation is driven by the interaction of the strong electric field induced between the electrodes with the heterogeneity in conductivity properties between the intracellular and extracellular spaces of the myocardium [8]. The VE effect has been used to explain the efficacy of defibrillation [9, 10, 11].

However, the requirement for high-energy (strong) defibrillation shocks, in order to ensure efficacy, used in ICDs results in limitations, such as reducing QOL (particularly in the event of inappropriate shocks) and limited battery life [12]. These clinical concerns have recently accelerated the quest to find lower-energy electrotherapy [13, 14, 15, 16]. Low energy protocols aim to apply several successive electrical shocks, with relatively small strength, achieving similar efficacy to strong defibrillation shocks for ATP-refractory VT episodes [16] and fibrillation [15, 17]. Despite their initial success, all protocols were delivered via conventional shock-vectors, and it remains unclear the mechanistic processes driving why the particular protocols used (often

[*]Corresponding author

✉ Shuang.qian@kcl.ac.uk (Qian)

ORCID(s): 0000-0002-2313-0268 (Qian)

highly complex) were more efficacious than others. A significant challenge therefore remains to better understand, optimise and personalise lower-energy shock protocols for ATP-refractory VTs in infarcted hearts to facilitate translation.

For decades, computational models have been widely applied to understand the mechanism of VT occurrences [18], simulate clinically-realistic defibrillation devices [19, 20, 21], optimise ATP protocols [22] and also in the design of novel electrode configurations [23, 24]. Modelling used in this context has significant utility in providing a carefully controlled, repeatable environment in which specific parameters may be tested and efficacies can be evaluated.

In this study, we present the use of biophysically-detailed simulation to evaluate the efficacy of two novel electrode configurations, which are suitable for patient-specific optimisation, against VT. Both configurations combine the concept of targeted shock delivery, based on *a priori* known VT substrate location, and low-energy electrotherapy. The first configuration is the "bipolar electrode" configuration, a conceptual configuration proposed by our group previously [23]. Unlike standard electrode placement in ICDs, this configuration does not have a can/ground placed outside of the heart. Instead, both positive and negative electrodes (localised in a specific alternating array) are placed inside the ventricular cavity which can provide directional stimulation to the specific region of tissue harbouring the centre of the reentrant circuit. This configuration also has the advantage of confining the electric field to the immediate vicinity of the heart, reducing the energy deposited outside of heart which is an important source of pains and discomfort in patients [25].

Secondly, we introduce a further novel configuration, termed the "transmural electrode" configuration. This, more clinically achievable and practical configuration, consists of two electrodes of opposite polarity - one intra-cavity, the other extra-cavity, producing a transmural field specifically targeted across the centre of reentrant circuit (critical isthmus (CI)). This configuration was conceived from the idea that any stimulus which simultaneously activates the CI (via the VE mechanism by applying opposite stimuli from either side) may be successful in efficiently terminating VT. This configuration aims to reduce the strength needed for electrotherapy by applying CI-targeted shocks.

These electrode configurations (bipolar and transmural) will be embedded within a cohort of high-resolution left ventricular (LV) porcine models constructed from *in vivo* magnetic resonance imaging (MRI) with a 1 mm isotropic resolution (not available clinically) to assess their efficacy against stable monomorphic VT. Specifically, models will be used to test the hypothesis that such targeted electrotherapy, delivered towards (bipolar) or 'through' (transmural) the scar substrate will terminate sustained VTs with greater efficacy compared to standard ATP and requiring considerably less than standard defibrillation shocks.

2. Methods

2.1. Geometrical models and Electrode Configurations

A cohort of infarct porcine finite element (FE) LV models were developed based on late-gadolinium enhanced cardiovascular MRI obtained seven weeks following myocardial infarction, as shown in Figure 1(a). Full details of the pipeline for image-based model construction has been described previously [18]. Briefly, images were segmented semi-automatically in the open source package Seg3D (www.seg3d.org) to delineate blood pool, myocardium, infarcted scar and border-zone (BZ) [26]. Tetrahedral FE meshes were created directly from the segmented images using CGAL library (https://www.cgal.org/), and smoothed using Meshtool [27]. All LV models were immersed within a cubic extracellular bath, as shown in Figure 1(a). Fibre architecture was incorporated using a rule-based approach [28].

The spacing between the electrodes are chosen to be the same as the length of the cubic electrodes which is because our previous study shows the total electrical flux is insensitive to the spacings of the bipolar electrodes [23] The arrangements and placements of the bipolar electrode configuration in all three LV models are shown in Figure 1(b). The electrode geometries were defined with Simpleware (Version P-2019.09; Synopsys, Inc., Mountain View, USA), constituting five cubes of size 4×4×4 mm^3 with 4 mm spacing, which is based on [23], but enlarged by a factor of 4 due to the smaller rabbit ventricles were used in this previous study. The spacing between the electrodes were chosen to be the same as the length of the cubic electrodes, as our previous study showed that the total electrical flux is insensitive to the spacings of the bipolar electrodes [23]. The bipolar electrodes were placed approximately in the middle of the LV cavity, aligned vertically, in order to enable its ability of target any area in the LV by switching the polarities of the surfaces [23]. In addition, they are placed sufficiently far from endocardial boundaries to minimize boundary effects. One of faces in the electrodes are orientated towards the scar region to provide targeted shock delivery. Following electrode placements, models were re-meshed in Simpleware to produce final average edge lengths of the 330 $\mu m \pm 25$ μm for myocardium, 600 $\mu m \pm 10$ μm for bath and 370 $\mu m \pm 10$ μm for bipolar electrodes. Note, the bipolar electrodes were defined as cubic regions within the bath space, and did not require specific re-meshing.
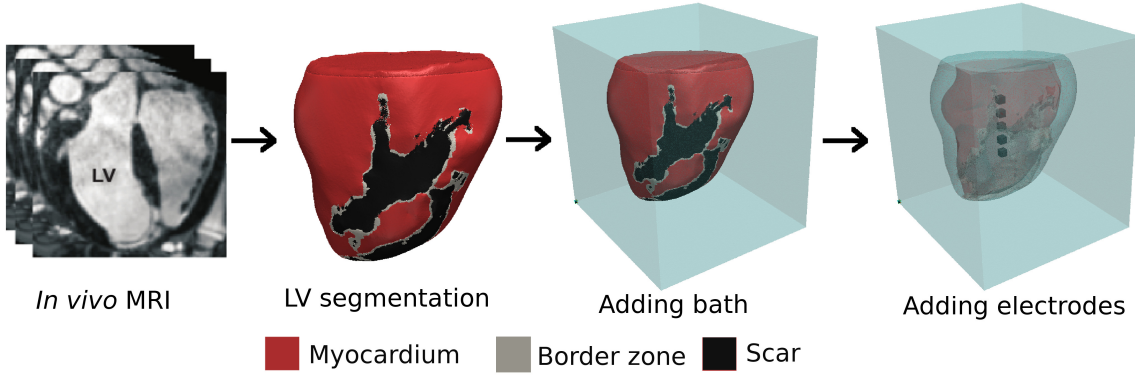
2.2. Biophysical model

Electrophysiological dynamics of the LV models were simulated using the Cardiac Arrhythmia Research Package [29] (https://carpentry.medunigraz.at/). The ventricular myocardium was represented by the bidomain equations [30]:
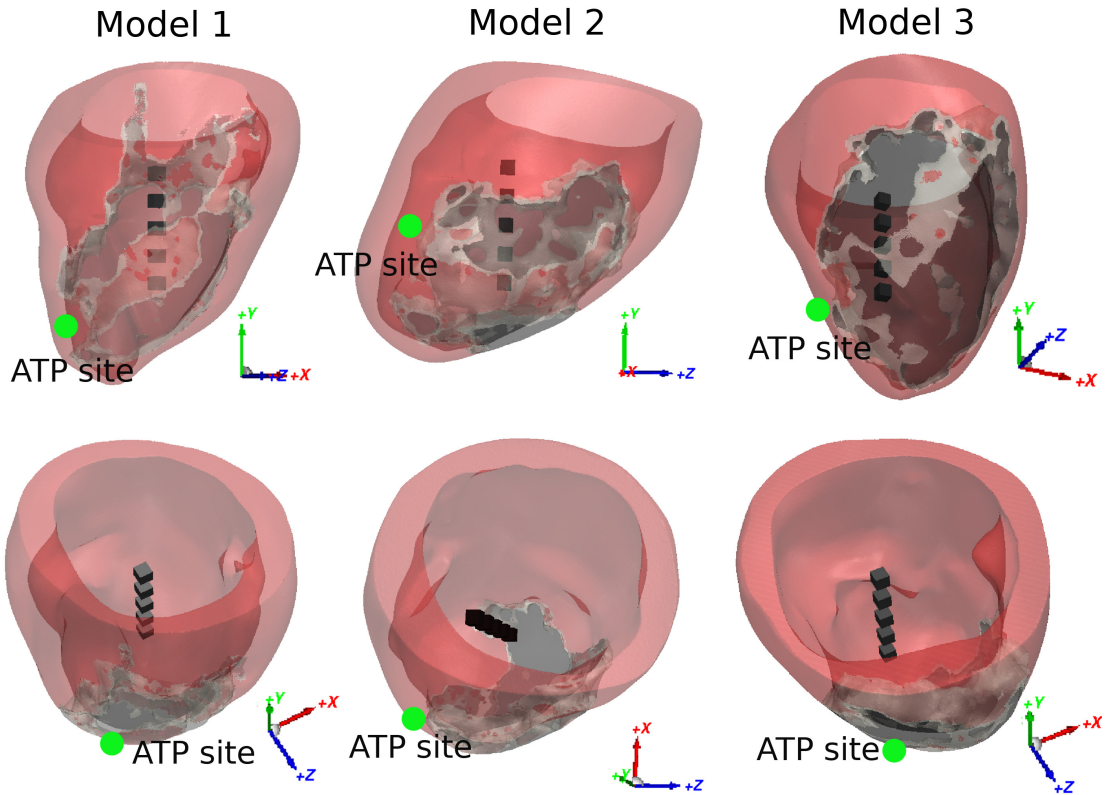
$$\nabla \cdot (\sigma_i \nabla \phi_i) = \beta I_m, \qquad (1)$$

$$-\nabla \cdot (\sigma_e \nabla \phi_e) = \beta (I_m - I_e), \qquad (2)$$

(a)

In vivo MRI   LV segmentation   Adding bath   Adding electrodes

■ Myocardium   ■ Border zone   ■ Scar

(b)

Figure 1: (a) Model generation pipeline of porcine LV meshes from *in vivo* MRI. (b) Placements of novel bipolar electrodes in the LV models, viewed from side and top. ATP delivery sites in all three LV models are marked with green dots which replicate the delivery site in clinical ICDs (apical septum of right ventricle).

where σ_i and σ_e are the intra- and extracellular conductivities, ϕ_i and ϕ_e are the intra- and extracellular electrical potentials, β is the surface area of membrane contained within a unit volume equal to $0.14 \ \mu m^{-1}$, I_m is the transmembrane current density and I_e is the extracellular stimulus current density. The transmembrane current density is given as:

$$I_m = C_m \frac{\partial V_m}{\partial t} + I_{ion}(V_m, \eta), \tag{3}$$

where C_m is the membrane capacitance per unit area, t is time and I_{ion} is the ionic current density depending on V_m

and η which is a vector of state variables describing channel gating and ionic concentrations. The transmembrane potential V_m is:

$$V_m = \phi_i - \phi_e \tag{4}$$

The extracellular bath is described as:

$$\nabla \cdot (\sigma_b \nabla \phi_b) = 0, \tag{5}$$

where σ_b is the extracellular bath conductivity and ϕ_b is the electrical potential in the bath space.

No flux conditions are imposed at the tissue and extracellular bath boundaries. while the flux is continuous between ϕ_e and ϕ_b:

$$\mathbf{n} \cdot (\sigma_b \nabla \phi_b) = \mathbf{n} \cdot (\sigma_e \nabla \phi_e), \tag{6}$$

$$\phi_b = \phi_e. \tag{7}$$

At the boundaries of extracellular bath, no flux condition is imposed.

Full bidomain simulations were performed during the electrotherapy delivery. During pre-conditioning (post-shock simulation), the more computationally efficient monodomain model was used:

$$\nabla \cdot (\sigma_m \nabla V_m) = \beta(I_m - I_s), \tag{8}$$

where σ_m is the harmonic mean conductivity tensor.

Anisotropic conductivity was assigned to reproduce the characteristic properties of myofibres. For the healthy tissue, the intra- and extra-cellular conductivities along the fibre direction were $\sigma_{il} = 0.174$ and $\sigma_{el} = 0.625 \ S/m$, while the intra and extra-cellular conductivities transverse to the fiber are $\sigma_{it} = 0.019$ and $\sigma_{et} = 0.236 \ S/m$ [31]. Based on our previous VT induction work [18], the conductivity for BZ tissue was set to be half of the conductivity for healthy tissue to simulate conduction slowing due to gap junction uncoupling and fibre disarray. The scar conductivity was set to 0.05 S/m, while the bath conductivity was set to 1 S/m, based on previous works [32, 33].

Ionic membrane dynamics (I_{ion}) in the porcine models was represented by Ten Tusscher (TT) model [34]. Based on ours previous works [18], the ionic properties in the health tissue were adjusted including 50% increase of the potassium currents I_{Kr} and I_{Ks} from the default settings of TT model to more accurate replicate the shorter porcine ventricular action potential duration (APD). In order to produce the substrates for block and reentry in the infarcted ventricle, the ionic properties in BZ were altered from health tissue including a 30%-65% reduction of the conductances of the potassium currents I_{Kr} and I_{Ks}, and 10%-90% reduction of the conductances of the sodium current I_{Na} based on ours [18] and other previous computational studies [22].

2.3. VT induction

Prior to tissue simulations, the single cell TT model was paced for 100 cycles at 2 Hz in order to produce stable single-cell states. These were saved and used as initial conditions for tissue simulations. Each LV model was paced either at the LV base or the LV apex in order to induce VT [18]. This involved three stimulus S1 at a basic cycle length of 500 ms, followed by S2 with a shorter coupling interval, reducing sequentially by 10 ms from 500 ms until unidirectional block was observed. If failure to capture occurred prior to unidirectional block occurring, another premature stimulus S3 was added which follows the same process until a block was achieved.

Following unidirectional block, in order to maintain the induced VT, the ionic properties in the BZ were adjusted to be the same as the ionic properties in the healthy tissue (as we have shown that longer APD in the BZ is in fact anti-arrhythmic, attenuating sustenance [18]). In addition, the conductivities in healthy tissue and BZ were adjusted, without altering their conduction velocities by more than 60% [22]. All induced VTs were then run for 3 cycles to ensure they were monomorphic and stable. After that, in order to generate a number of VT episodes with various VT cycle lengths (VTCLs), we adjusted conductivities and ionic properties in BZ as in [18, 22]. The ionic properties in the BZ were altered including a 30%-65% reduction of the conductances of the potassium currents I_{Kr} and I_{Ks}, and 10%-90% reduction of the conductances of the sodium current I_{Na}. The conductivities were adjusted without varying conduction velocity by more than 10%. Each VT episode was simulated for more than five cycles to ensure it was stable and monomorphic before applying electrotherapy.

In total, 40 separate VT episodes were generated within three LV models with their VTCLs ranging from 260 ms to 530 ms as shown in Figure 2, including 7 fast VTs (VTCL $\leq$ 320 ms) and 33 slow VTs (VTCL > 320 ms). Next, three different electrotherapy protocols were applied to each of the 40 VT episodes independently and their efficacy evaluated. Specifically, ATP was compared to single shocks delivered from the bipolar electrode configuration and from the transmural electrode configuration.
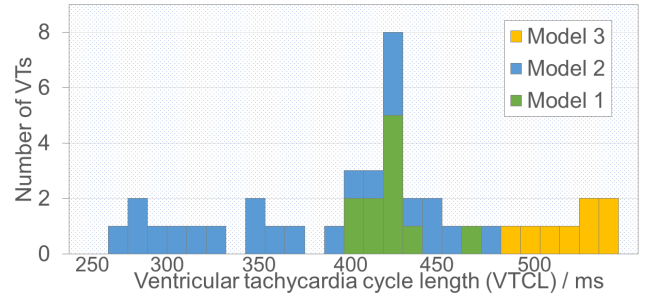
Figure 2: The ventricular tachycardia cycle lengths (VTCLs) histogram

2.4. ATP protocols

Traditional burst ATP therapy was delivered from a septal location near the apex of the LV (RV side), as shown in Figure 1(b). Note that the scar regions in all three LV models are located proximal to the ATP delivery site. The burst ATP protocol consisted of 2 sequences of 8 pacing pulses with an equal inter-stimulus interval pacing at 88% of the VTCL. In the 2nd sequence, the pacing interval was decreased by 10 ms. The initial pacing start timing was calculated as the time at 88% of the VTCL after the last activation was detected at the pacing location. The stimulus current was 50 $\mu A/cm^2$, delivered to a volume of $5 \times 5 \times 5 \ mm^3$, replicating the pacing delivered from the ICD lead.
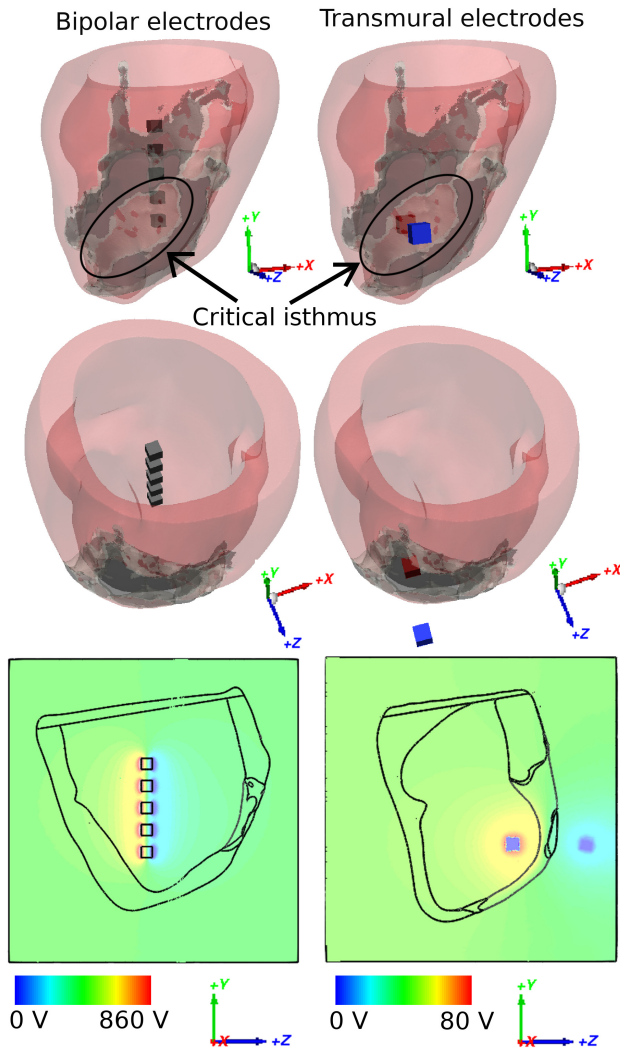
Figure 3: Bipolar and transmural electrode configurations and field distributions. Bipolar electrode (left, black) and transmural electrode (right, blue and red) configurations in Model 1 shown in side and top views. The clipping images shows the extracellular potential distribution during stimulus delivery.

2.5. Bipolar/Transmural electrode configurations and electrotherapy protocols

Both the bipolar and transmural electrode configurations simulated here are designed to deliver the stimulus to the centre of the re-entrant circuit, through the CI to perform targeted electrotherapy, as shown in Figure 3. In the bipolar electrode configuration, the ground electrode ($0\ V$) was assigned to the faces near the CI, and applied voltages assigned to the opposite faces, as shown in the clipping images of Figure 3. As discussed previously, the bipolar configuration constitutes five cubes of size $4{\times}4{\times}4\ mm^3$ with $4\ mm$ spacing [23], aligned vertically, approximately in the middle of the LV cavity. In the transmural configuration, the positive electrode is assigned to be inside the LV blood pool, and ground outside of LV within the RV blood pool. The transmural electrodes consist of two cubic electrodes with

the side-length $5\ mm$. Both electrodes are placed close to the centre of the CI with the minimum distance to cardiac tissue of approximately $1\ cm$.

The electrotherapy protocols of both novel electrode configurations were first tested on a smaller cohort of 6 VTs, in order to choose an optimal stimulus delivery time and minimum strength needed for terminating VT. The duration of the stimulus applied via both transmural and bipolar configurations was fixed at $5\ ms$ and the strength varied in steps of $20\ V$ in the bipolar case and steps of $10\ V$ in the transmural case. The stimulus was applied at different timings, defined as a percentage of the VTCL since the last activation detected at the CI. Based on the success of electrotherapy applied by each respective configuration upon the 6 initial VT episodes, we chose an optimal electrotherapy setup in terms of delivery time and strength. Specifically, two strengths were chosen in order to compare the two novel configurations with different goal efficacies: the first strength (termed S_{pEff}) was defined as the stimulus strength which was seen to achieve a partially high efficacy at 5 out of 6 of the tested VTs; the second strength (termed S_{fEff}) was defined as the stimulus strength which was seen to achieve full efficacy of 6 out of 6 of the tested VTs.

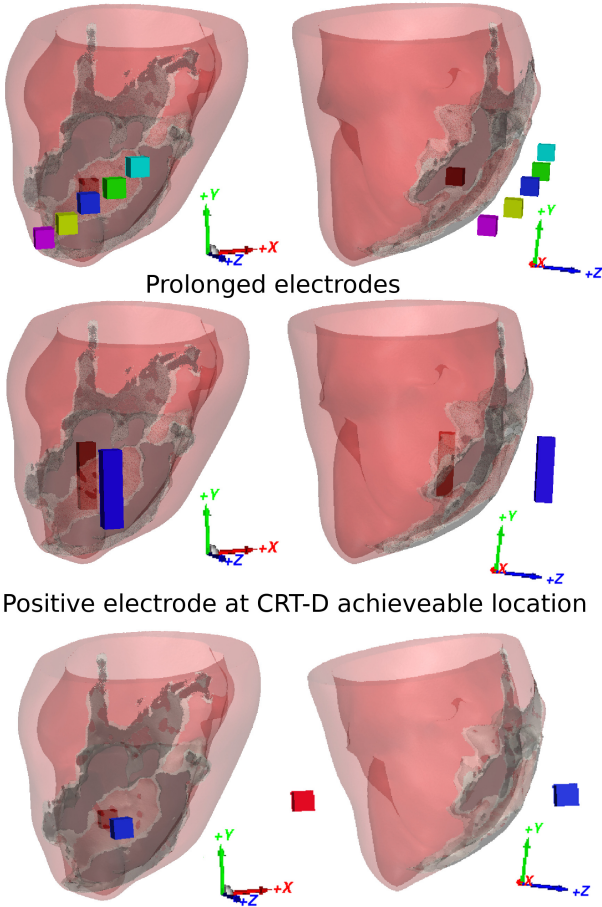## 2.6. Sensitivity of Transmural Electrode Configuration

The practical clinical translation of the transmural electrode configuration proposed here may encounter alterations, such as viability in the specific placement of electrodes, electrode size. We therefore conducted three sensitivity tests of shock vectors in the transmural electrode configuration, as shown in Figure 4, applied to a smaller cohort of three VTs (one from each LV model). The first test was designed to vary the locations of electrodes with respect to the scar locations whereby the positive electrode inside the cavity remains fixed, whilst the ground electrode outside of LV was varied to five locations in three models, covering all regions along the length of the CI, giving 15 scenarios. Note that the middle location, shown in blue in Figure 4, is same as the setup used in the default setup.

The second test was designed to increase the size of both electrodes, more similar to the length of the RV coil in clinical ICDs. As is shown in Figure 4, both electrodes were prolonged by $20\ mm$, and their placements were adjusted accordingly to make sure the centroids of both electrodes were still in line with the centre of the CI, giving 3 scenarios.

The final test involved moving the positive electrode (originally placed inside the LV blood pool) to now be outside of the LV, while maintaining the shock vector to be still through the CI. This new location may be more representative of a potential shock vector between an RV electrode and and LV coronary sinus electrode in a clinical cardiac resynchronization therapy defibrillator (CRT-D) device.

In all tests, a single stimulus using S_{fEff} was applied to all three VTs tested.

Varying the ground electrode out of LV around scar

Prolonged electrodes

Positive electrode at CRT-D achieveable location

Figure 4: Sensitivity tests setup of the transmural electrode configurations shown in direct (left) and side (right) views. First test (top) varies the location of the ground electrode (outside the LV) in 5 different locations. The middle blue electrode represents the same location as the default setup. Second test (centre) shows the prolongation of the transmural electrodes. Third test (bottom) shows the movement of the positive electrode to be outside of the LV cavity, which maintains a shock vector through the CI.

3. Results

3.1. Dynamics of induced VTs

Three example of slow VTs in each model and one fast VT in Model 2 are shown in Figure 5. The VTCL of Model 3 is seen to be long because of the slow conduction in the CI which, in this model, represents a relatively long, thin anatomical pathway, combined with the fact that the entire CI region in Model 3 is BZ, unlike the other two models in which the CI regions are largely composed of healthy myocardium. The fast VT in Model 2 has a much shorter VTCL which is due to the correspondingly shorter VT reentrant pathway. As shown in Figure 5, comparing with the slow VT in Model 2, the fast VT circulates in approximately half of the CI.

3.2. Optimal electrotherapy protocols for bipolar and transmural electrode configurations

Different delivery timings and shock strengths were applied to a smaller cohort of 6 VT cases using both the transmural and bipolar electrode configurations in order to find the optimal delivery protocol for each case, as described in the Methods 2.5. As shown in Figure 6, for the bipolar configuration (blue line), with increasing delivery time (later from the timing of the last activation), the average minimum shock strength needed for terminating (all 6) VTs decreases
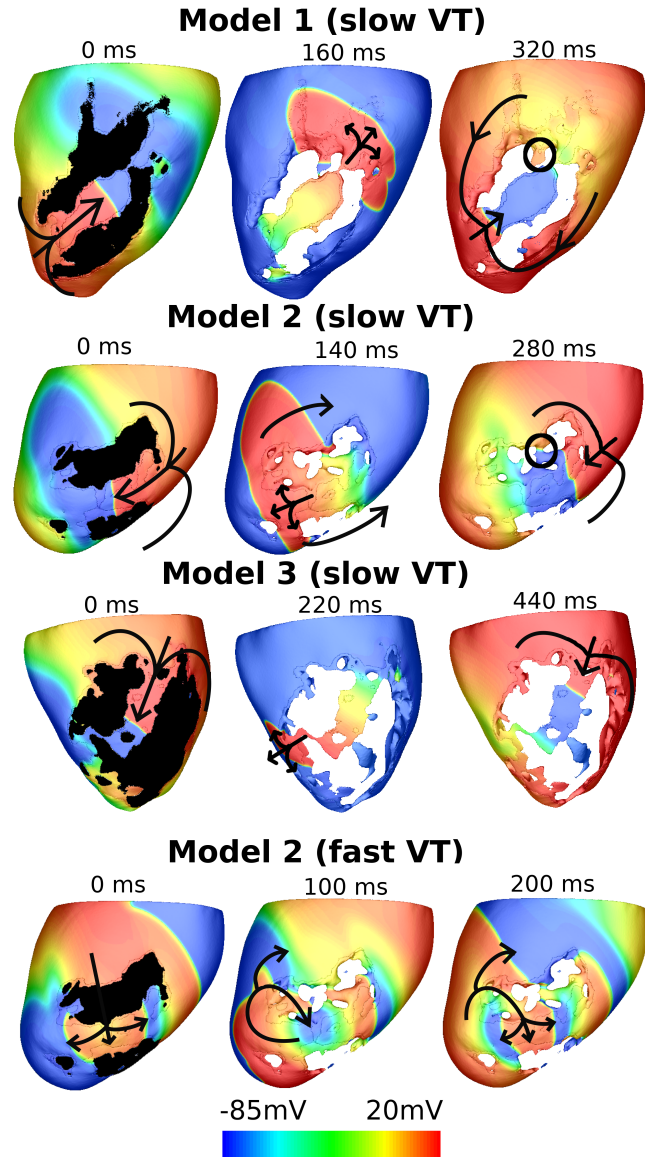
Figure 5: Transmembrane potential (V_m) maps of at different timings during slow VTs induced in Model 1, 2 and 3, along with a fast VT induced in Model 2. VTCLs are 400 ms, 350 ms, 530 ms and 270 ms. Only the first time plots show the scar region while the others are removed in order to clearly show the pathway of activation wave. The black arrows show the propagation direction of the VT through the CI. The black circles mark the small extra pathways at the exit of the CI in Model 1 and 2.

rapidly. At the latest delivery time of 88% VTCL (since the last sensed activation), the smallest average strength is achieved at 700 V. However, the effect of pacing times on the minimum shock strength in the transmural configuration (red line) is more subtle. The average strength at different delivery timings ranges from 45 V to 63 V, with a small variation of less than 20 V. The full results detailing the individual strengths required to terminate all 6 VTs are shown in Appendix Figure S1.
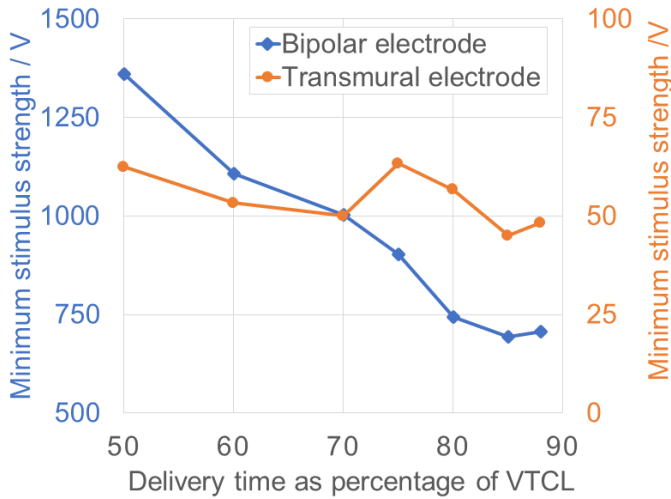

Figure 6: Average minimum stimulus strength needed, for terminating VT with the bipolar (left blue line) and transmural (right red line) electrode configurations, is plotted against the shock delivery time defined as the percentage of the VTCL since the last activation detected at the CI. Note that at 50% and 60% of VTCL, some VTs failed to terminate with the maximum delivered stimulus. In these cases, the average value is calculated by eliminating those unsuccessful cases.

Based on Figure 6, we decided to use a delivery timing of 88% of the VTCL in both electrode configurations moving forward, as the average shock strength needed at this delivery time is relatively lower than the other times, and is also the same as used in ATP therapy. As shown in Appendix Figure S1(a), application strengths S_{pEff} and S_{fEff} are 860 and 1700 V for the bipolar configuration, whereas for the transmural configuration are 80 and 120 V as in Appendix Figure S1(b).

Figure 7(a) highlights the mechanism by which a VT is terminated by the bipolar configuration using the larger shock strength S_{fEff} (1700 V), compared with the same VT that is not terminated by using the weaker strength S_{pEff} (860 V). In both cases, the Figure shows that at time 5 ms when the stimulus just ends, most of the area at the endocardium around the CI is depolarized, while most of the area at the epicardium near the CI is hyperpolarized. However, as shown in the two enlarged images, there is less depolarised tissue area seen on the endocardium within the CI in Figure 7(b), compared to Figure 7(a) because of the relatively smaller stimulus strength in this case. Consequently, the tissue near the tail of the CI remains excitable, so at time 245 ms it becomes depolarized by a remnant VT wavefront and the VT is not terminated.
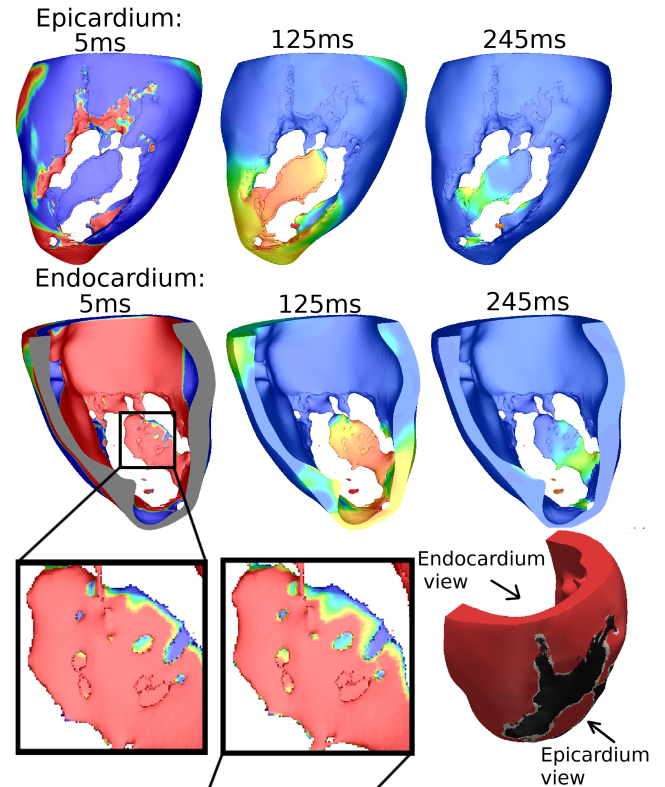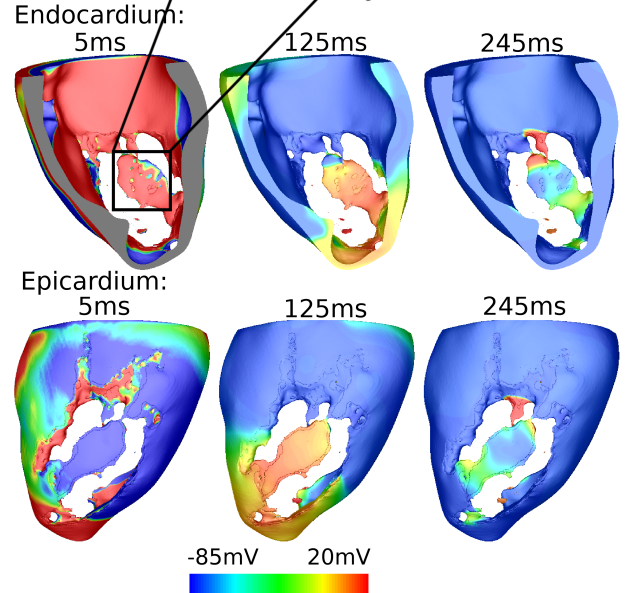
Figure 7: Transmembrane potential (V_m) distributions during shock application with the bipolar electrode configuration showing successful (panel a) and unsuccessful (panel b) VT termination using strength S_{fEff} and strength S_{pEff}, respectively in Model 1. Note that the stimulus applied by the bipolar electrodes starts at 88% VTCL in the CI location, as shown in Figure 3 and lasts for 5 ms. Two views are shown from the epicardium and the endocardium of the LV. Enlarged views of the CI region are marked by blacked rectangles.
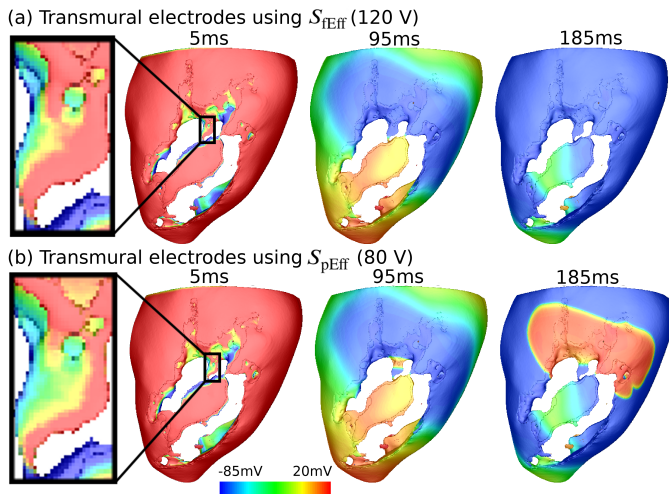
Figure 8: Transmembrane potential (V_m) distributions during shock application with the transmural electrode configuration showing successful (panel a) and unsuccessful (panel b) VT termination using strength S_{fEff} and strength S_{pEff}, respectively in Model 1. Note that the stimulus applied by the tranmural electrodes starts at 88% VTCL in the CI location, as shown in Figure 3 and lasts for 5 ms. Two views are shown from the epicardium and the endocardium of the LV. Enlarged views of the CI region are marked by blacked rectangles.

Figure 8(a) highlights the mechanism by which a VT is terminated by the transmural configuration using the larger shock strength S_{fEff} (120 V), compared with the same VT that is not terminated by using the weaker strength S_{pEff} (80 V). In both cases, at time 5 ms a large area of epicardium near the top of the CI is depolarized due to the stimulus. As shown in the two enlarged images, the larger stimulus strength in Figure 8(a) results in depolarization of more area at the small pathway at the mouth of the CI which successfully prevents the propagation of excitation from this pathway, terminating the VT. In contrast, the weaker strength of stimulus in Figure 8(b) leaves a larger excitable area within this critical area, which is not sufficient to block the remaining VT wavefronts, and reentry continues.

3.3. Efficacy of two novel electrodes configurations comparing with ATP

Figure 9(a) shows the efficacy of the bipolar and transmural electrode configurations for both shock strengths (S_{fEff} and S_{pEff}) applied to all 40 VT episodes, in comparison with success of ATP. The Figure shows that the efficacy of both electrode configurations using either stimulus strength is higher in comparison to the efficacy of ATP (45%). Furthermore, the efficacy of both novel configurations is seen to improve with the increase of shock strength, S_{fEff} vs S_{pEff}. The efficacy of the bipolar configuration is increased from 63% using strength S_{pEff} (860 V) to 93% using strength S_{fEff} (1700 V), while the efficacy of the transmural configuration is increased from 70% using strength S_{pEff} (80 V) to 85% using strength S_{fEff} (120 V). Efficacies of bipolar and transmural configurations using strength S_{fEff} on slow

and fast VTs are compared in Figure 9(b). The Figure shows that both novel electrode configurations are more efficient at terminating slow VTs, compared to fast VTs. The efficacy for slow VTs is seen to be as high as 100% for the bipolar configuration and 97% for the transmural configuration. Furthermore, the efficacy of the bipolar configuration for fast VTs (57%) is seen to be higher than for the transmural configuration (29%).

(a)

(b)
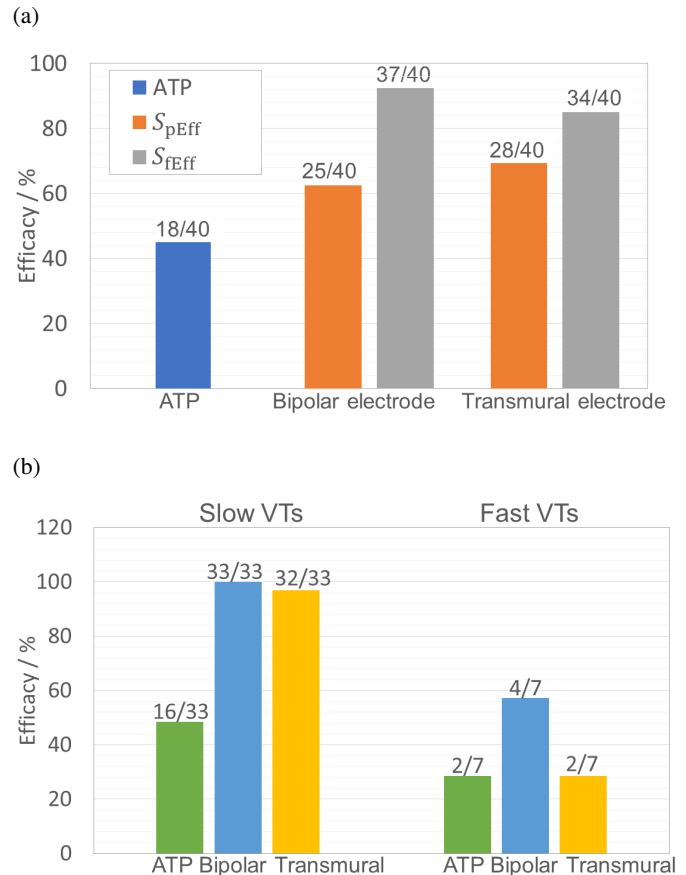
Figure 9: (a) Comparison of the efficacy of the bipolar and transmural electrode configurations with ATP, applied to all 40 VT episodes. Strengths S_{pEff} and S_{fEff} for bipolar configuration are 860 V and 1700 V. Strengths S_{pEff} and S_{fEff} for transmural configuration are 80 V and 120 V. (b) Comparison of the efficacies of bipolar and transmural electrodes using strength S_{fEff} with ATP, on slow and fast VTs separately.

3.4. Sensitivity analysis for transmural electrode placements and geometries

Three sensitivity tests examining the specific placements and geometries of the transmural configuration (as described in the Methods 2.6) were conducted on a smaller cohort of three VTs (one from each LV model). The respective efficacies for terminating VTs for each variation are shown in Figure 10. The Figure shows that varying the placement (test 1) of the ground electrodes at the outside of the LV results in a slight reduction of efficacy to 73%, comparing with the efficacy of previous fixed placements of the transmural
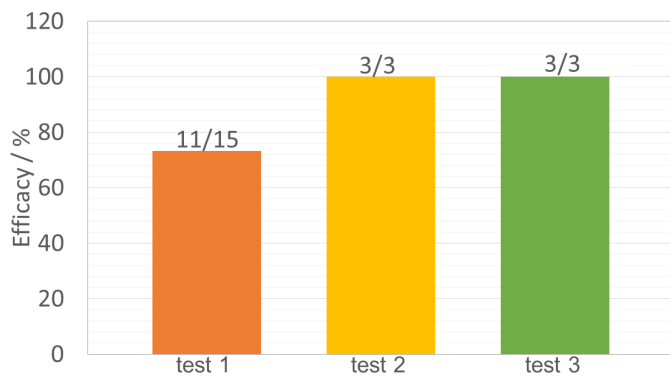
Figure 10: Sensitivity analysis of the specific placements and geometry of the transmural electrode configuration, tested on a smaller cohort of 3 VT episodes (one from each LV model). Test 1 varies the placement of the ground electrode outside of the LV to five locations around the CI (5 cases). Test 2 prolongs the electrodes size (3 cases). Test 3 moves the positive electrode outside of the LV cavity, whilst maintaining the shock vector through the CI (3 cases). All stimulus strengths used here are S_{fEff}.

electrodes (85%). The Figure also shows that the efficacy of the transmural configuration is relatively insensitive to a change in electrode geometry (test 2) or moving the positive electrode outside of the LV cavity (test 3), as the efficacies of these tests remain high at 100%.

4. Discussion

In this virtual study, we tested the efficacy for VT termination of two novel electrode configurations (bipolar and transmural) and compared with conventional ATP using a cohort of infarcted LV porcine models. In our previous work [23], we introduced the novel bipolar electrode configuration and explored its effect on stimulating passive myocardial tissue in realistic (rabbit) cardiac models. In this study, we further assess its electrotherapy efficacy, in addition to our new transmural electrode configuration, using a comprehensive library of sustained VT episodes and compare against traditional ATP. Here, we have demonstrated that both configurations are highly effective at terminating VTs. Specifically, we demonstrate that the efficacy of bipolar and transmural configurations are 93% and 85%, higher than 45% for ATP. Both novel electrode configurations are able to provide infarct-targeted electrotherapy, focussing the applied field on the core of the reentrant circuit sustaining the VT, consequently minimising the energy required for VT termination and potentially reducing pain due to extra-cardiac stimulation. Importantly, we highlight the mechanism of VT termination by both novel electrode configurations (Figure 7 and 8) to be targeting the core of re-entrant circuit (the CI) causing depolarisation which results in functional block that stops the propagation of the VT. Our findings reveal the significant potential of these low-energy targeted electrotherapy strategies, guiding future pre-clinical or clinical testing and development.

4.1. Utility of our virtual 'library' of simulated VT episodes

The VTs in this study were induced by similar protocols used in other recent computational modelling studies [18, 22]. Similar to these other works [22], in our simulations we found that the fast VTs were difficult to induce, as the excitable gap is small in such cases and the VTs are often induced but self-terminated. Interestingly, we found that the VTCLs varied significantly between models, which was mainly seen to be dependent on the explicit infarct anatomies and the CI. As shown in Figure 2, the VTCLs in Model 3 are generally longer than the other two models, which appears to be largely driven by the long CI of Model 3 which is mainly composed of slow conducting BZ tissue (Figure 1(b) and 5). It is also shown in Figure 5 that multiple pathways through the scar in Model 2 may generate 'short-circuit' effects leading to both fast and slow VTs in the same model. This demonstrates how the complex structure of the scar may dictate the specific VT substrate, and emphasises the utility of our high-resolution pre-clinical model cohort in being able to simulate these important aspects. Considering the VTCLs of our induced VTs are within the range of clinically recorded VTs, the variation of VTCLs between models, and the detailed representation of the VT substrate, provides a robust library of VT episodes with which to test electrotherapy efficacy.

4.2. Mechanistic dependence of novel electrotherapy configurations upon stimulus timing

Current ATP protocols use a variety of pacing times, ranging from 75% to 91% of VTCL [5, 35, 36], with little mechanistic understanding regarding the optimal value. Therefore, we conducted a grid search of the minimum stimulus strength required for VT termination for different pacing times (% of VTCL) for our bipolar and transmural electrode configurations.

We found a descending trend of minimum strength as the application times increase for the bipolar configuration (Figure 6). A much larger shock is required if the application time is too early, as more targeted tissue is not fully repolarised. However, applying the stimulus at timings later than 80% of VTCL showed little difference in the strength required. In contrast, for the transmural configuration, little correlation between stimulus time and the minimum strength required for VT termination was found (Figure 6).

In comparison to the bipolar electrode configuration, the transmural electrodes are situated much closer to the centre of CI and both electrodes are placed at opposite sides of the CI, which enables delivery of more energy to the targeted tissue (i.e. through the volume of the CI). We postulate that the transmural current path setup by the transmural electrode configuration is crucial to its success, inducing as it does, a strong virtual electrode response from the epicardial and endocardial tissue of the CI. Furthermore, the more concentrated field induced by the transmural configuration results in a stronger localised tissue response within the CI,

enough to override the difference in the area of repolarised tissue due to pacing times. Finally, it is also interesting to note that the range of strengths needed for different VT episodes are large: up to 1500 V in the bipolar and 120 V in the transmural configuration. This suggests that personalising electrotherapy based on the prior information of anatomical structure and electrophysiology properties could improve efficacy of electrotherapy and QOL by deceasing unnecessary high shock voltage.

4.3. Energy requirement for novel configurations

The Defibrillation Threshold (DFT) is a conventional clinical metric in assessing ICD efficacy, which can be defined as the lowest energy required to successfully defibrillate. Current ICDs are usually programmed to deliver a first shock of 20-35 J energy, with additional stronger shocks if the first attempt fails [37, 38]. The maximum defibrillation energy varies in patients and devices, typically being somewhat higher in subcutaneous ICD devices, but can reach up to 360 J [39]. To allow direct comparison with current ICDs, we estimated the approximate energy required for successful therapy for our two novel electrode configurations using similar methods as in our previous study [21] (based-on capacitive discharge): the energy required for the bipolar configuration is approximately 37 J for 860 V shock yielding 63% efficacy and 145 J for 1700 V shock yielding 93% efficacy. Although this energy is slightly higher than the current conventional ICDs, it should be noted that unlike the conventional ICDs with an extra-cardiac can placed under the clavicle, this configuration has all electrodes placed within the LV cavity. The electric field generated by these electrodes also decays rapidly with the increasing distance from the source. Consequently, the majority of the regions of high electric field are confined within the LV, thus, the energy delivered by the device (which is higher than standard ICD programming), is confined within the heart (where it is needed), potentially reducing the pain in patients due to stimulation of extra-cardiac tissues and organs.

However, the energy required for the transmural electrode configurations is 0.32 J for 80 V shock yielding 70% efficacy which increases to 0.72 J for 120 V shock yielding 85% efficacy, which is two orders of magnitude *lower* than conventional ICDs. In the transmural electrode configuration, the positive and ground electrodes are placed across the centre of reentrant circuit (CI) and also very close to each other which results in a short current path. The resulting low impedance and high voltage gradient generates more stronger VE effects, and importantly, focussed to the critical region of tissue to facilitate interruption of the reentrant circuit. Thus, only a small amount of energy is required for VT termination.

Moreover, we also show that both novel electrode configurations are more efficient, as only one single shock/stimulus is required to achieve a higher efficacy of VT termination comparing with the traditional ATP, in which multiple pacing stimulus and even multiple sequences of stimulus are required.

4.4. Efficacy for fast VTs

ATP is known to be found less efficient for fast VTs, compared with slow VTs, which we also found in this study. Interestingly, we also found a similar result of both novel electrode configurations. Both novel configurations were seen to be more efficient on slow VTs (efficacy of 100% and 97% for bipolar and transmural configurations, respectively), while the efficacy on fast VTs was much lower (57% and 29% in bipolar and transmural configurations, respectively). Interestingly, the bipolar configuration significantly outperformed the transmural configuration for fast VTs, whereas the transmural configuration performed similar to ATP in this case.

Fast VTs are known to have a smaller excitable gap, compared to slower VTs, making it harder for ATP to both capture and also successfully penetrate and close this gap for VT termination. The same in true for the novel electrode configurations, particularly for single shocks, as delivered here, which explains the significantly reduced efficacy in our novel configurations when applied to fast VTs (Figure 9). In this work, we presented use of one single monophasic shock delivered from both novel electrodes configurations, as this was effective for initial evaluation of efficacy and more effective dissection of the mechanisms of terminating VTs. This is in contrast to recent low-energy electrotherapy research involving multiple shocks/stimulus in rather complex and non-intuitive protocols [14, 16]. Moving forwards, our configurations may be used in conjunction with more complex shock/stimulus sequences to further enhance electrotherapy efficacy for monomorphic VTs (as tested here) and potentially also polymorphic VTs and VF.

4.5. Sensitivity analysis of the placement of transmural electrodes

The sensitivity tests of transmural electrodes are conducted in this study to investigate its feasibility and reliability for clinical usage in the future. We found that varying the location of ground electrodes reduces the efficacy of VT termination slightly to be 73% from 85%. This small decrease of efficacy is due to the difference in the placement of the ground electrode, producing different shock vectors which in turn affects the targeted area. As shown in Figure 8 (a), for the transmural configuration, VT is terminated because the shock depolarizes a critical area of myocardium in the CI which prevents further VT propagation. In cases with different ground electrode placements, the critical area may not be fully depolarized by the altered shock vector, which could result in failure to terminate. The effect of electrode location can be controlled by carefully placing the electrodes with the aid of prior knowledge of VT substrate regions.

Instead of placing the electrodes at an optimal location, we also showed that a potentially more straightforward approach to ensure robustness of the transmural configuration may be to use larger electrodes i.e. the extended electrodes shown in Figure 4, similar to a conventional coil used in ICDs. In addition, we also tested the case in which the

ground electrode were moved out of the LV blood pool, while maintaining the shock vector targeted at the centre of the CI, which still ensured 100% efficacy on the small test cohort. Such a setup may be more achievable than having an electrode in the LV, utilising conventional RV electrodes and multipolar electrodes in LV veins of a CRT-D device.

4.6. Practical clinical utility of novel designs

In order to utilise the ability of directional stimulation of both novel electrodes, it is important to know approximate location of the VT substrate prior to implantation. Imaging techniques, such as contrast-enhanced MRI is the most commonly-used method to obtain such information. There are also clinical algorithms which can predict the approximate VT exit sites based on the electrocardiograms of VT [40]. Furthermore, we are currently working on real-time automated identification of VT locations using electrograms (EGMs) recorded from ICDs [41].

The bipolar electrode configuration has more complex electrodes which may require more radical overhaul of current clinical ICD electrode design and manufacture. However, this configuration may be modified as a single lead, where all the conducting surfaces are placed, similar to current RV coils used in present ICDs. Furthermore, similar bipolar designs with directional capability also exist in brain stimulation [42, 43], demonstrating the potential feasibility to further our designs in the setting of cardiac electrotherapy. Practically placing a lead in the LV may be problematic due to implantation complexities and associated increasing risks of blood clot formation. In this cases, our bipolar configuration may also be placed in the RV which will still be effective to septal VTs, as shown in this study. For VTs in other locations of the LV, may still deliver directional shocking, albeit at an additional distance.

In contrast, the transmural electrode represents a more clinically translatable design in the short-term, as it may be incorporated into the design of current clinical devices (CRT-Ds), as shown in Figure 4, utilising the RV coil and electrodes in the lead within the LV vein (coronary sinus). Moreover, novel designs are emerging which show the potential for transmural configurations to be further developed. For example, [44, 45, 46, 47] describe novel electrotherapy electrode designs that are able to attach to the epicardial surface of the heart to provide highly localised electrical recording and stimulation. Such flexible electrodes may provide the distal electrode (outside the heart) in our transmural configuration, with the dis-similar intra-cavity electrode provided by a standard RV-coil electrode (as tested in our sensitivity analysis).

4.7. Limitations and future work

In this study we used a human ventricular ionic cell model, adjusted to replicate the expected porcine action potential duration. This was due to the absence of a porcine-specific cell model at the time the study was conducted. Unfortunately, it was not possible to perform the study with a cohort of human ventricular anatomical models, due to difficulties in obtaining high-resolution MRI of infarct

patients of sufficient quality for detailed model construction. As mentioned, the ability of our models to faithfully reconstruct the detailed structural anatomy of the scar and BZ was essential for accurate representation of infarct-driven VT dynamics and would not have been possible with clinical data at the present time. Secondly, this study has a relatively small cohort of three porcine models (as monomorphic VT was non-inducible in the other four porcine models that are also developed in the same pipeline as shown in Figure 1(a)). However, we were able to increase the variety of induced VT episodes in our 3 models by tuning EP properties, enabling both fast and slow VTs with a range of VTCLs observed clinically to be simulated (as in [22]). Thirdly, the scar regions in all three pig models was located near the septum, due to the specific infarct-induction procedure applied experimentally. The ATP delivery sites in this study were chosen as those commonly used in ICDs, delivered through the RV lead placed close to the septum near the apex. In reality, the scar can be located in a range of locations throughout both the LV, RV and septum. However, we believe that, as our novel configurations are ultimately designed to target the specific substrate sustaining the VT, assessing their efficacy in the models used here represents a robust approach.

The next step of this study will be to conduct rigorous experimental validation, which would pave the way to further optimisation of the proposed designs for manufacturing and production. The simulation work conducted here circumvents many inherent experimental limitations in performing such investigations (for example, difficulties in inducing stable, monomorphic VT, issues with fabricating bespoke electrode designs) and thus provides much utility to focus and refine the experimental parameters to be investigated and the scope of the experiments undertaken.

5. Conclusion

Two novel electrode configurations are proposed here that have the ability to deliver directional stimulation to the centre of a reentrant circuit, enhancing electrotherapy efficacy for VT termination, above conventional VT, tested on an in silico cohort of porcine infarcted LV models. The bipolar electrode configuration is able to confine the majority of the electric field within the heart, requiring similar shock energies to conventional ICD biphasic shocks, though importantly whilst reducing deposition of energy outside of the heart, potentially reducing unwanted ICD pain and side-effects. Our novel proposed transmural electrode configuration places electrodes physically closer to the targeted tissue, therefore able to achieve a very high efficacy with delivered energy two orders of magnitude lower than conventional ICD defibrillation. This work opens-up opportunities for further direct manufacture and experimental testing, as well as further in silico optimisation and testing, of these novel designs.

Declaration of competing interest

The authors declare that there is no conflict of interest.

Acknowledgment

References

[1] J. A. Ezekowitz, P. W. Armstrong, F. A. McAlister, Implantable Cardioverter Defibrillators in Primary and Secondary Prevention: A Systematic Review of Randomized, Controlled Trials, Annals of Internal Medicine 138 (2003) 445–53.

[2] H. C. Kamphuis, J. R. de Leeuw, R. Derksen, R. N. Hauer, J. A. Winnubst, Implantable cardioverter defibrillator recipients: Quality of life in recipients with and without ICD shock delivery: A prospective study, Europace 5 (2003) 381–9.

[3] J. Tomzik, K. C. Koltermann, M. Zabel, S. N. Willich, T. Reinhold, Quality of Life in Patients with an Implantable Cardioverter Defibrillator: A Systematic Review, Frontiers in Cardiovascular Medicine 2 (2015).

[4] M. O. Sweeney, L. Sherfesee, P. J. DeGroot, M. S. Wathen, B. L. Wilkoff, Differences in effects of electrical therapy type for ventricular arrhythmias on mortality in implantable cardioverter-defibrillator patients, Heart Rhythm 7 (2010) 353–60.

[5] M. O. Sweeney, Antitachycardia pacing for ventricular tachycardia using implantable cardioverter defibrillators: Substrates, methods, and clinical experience, PACE - Pacing and Clinical Electrophysiology 27 (2004) 1292–305.

[6] M. Santini, M. Lunati, P. Defaye, J. Mermi, A. Proclemer, S. Del Castillo-Arroys, G. Molon, E. Santi, T. De Santo, X. Navarro, A. Kloppe, Prospective multicenter randomized trial of fast ventricular tachycardia termination by prolonged versus conventional antitachyarrhythmia burst pacing in implantable cardioverter-defibrillator patients-Atp deliVery for pAiNless ICD thErapy (ADVANCE-D) trial results, Journal of Interventional Cardiac Electrophysiology 27 (2010) 127–35.

[7] M. M. Gulizia, L. Piraino, M. Scherillo, C. Puntrello, C. Vasco, M. C. Scianaro, F. Mascia, O. Pensabene, S. Giglia, G. Chiarandà, I. Vaccaro, S. Mangiameli, D. Corrao, E. Santi, A. Grammatico, A randomized study to compare ramp versus burst antitachycardia pacing therapies to treat fast ventricular tachyarrhythmias in patients with implantable cardioverter defibrillators: The PITAGORA ICD trial, Circulation: Arrhythmia and Electrophysiology 2 (2009) 146–53.

[8] I. R. Efimov, M. W. Kroll, P. J. Tchou, Cardiac bioelectric therapy: Mechanisms and practical implications, 2009.

[9] I. R. Efimov, F. Aguel, Y. Cheng, B. Wollenzier, N. Trayanova, Virtual electrode polarization in the far field: Implications for external defibrillation, American Journal of Physiology - Heart and Circulatory Physiology 279 (2000) 1055–70.

[10] O. F. Sharifov, V. G. Fast, Role of intramural virtual electrodes in shock-induced activation of left ventricle: Optical measurements from the intact epicardial surface, Heart Rhythm 3 (2006) 1063–73.

[11] A. Connolly, E. Vigmond, M. Bishop, Virtual electrodes around anatomical structures and their roles in defibrillation, PLoS ONE 12 (2017) 1–19.

[12] A. S. Manolis, T. Maounis, S. Koulouris, V. Vassilikos, âĂIJReal lifeâĂİ longevity of implantable cardioverter-defibrillator devices, Clinical Cardiology 40 (2017) 759–64.

[13] S. W. Morgan, G. Plank, I. V. Biktasheva, V. N. Biktashev, Low energy defibrillation in human cardiac tissue: A simulation study, Biophysical Journal 96 (2009) 1364–73.

[14] L. J. Rantner, B. M. Tice, N. A. Trayanova, Terminating ventricular tachyarrhythmias using far-field low-voltage stimuli: Mechanisms and delivery protocols, Heart Rhythm 10 (2013) 1209–17.

[15] Y. C. Ji, I. Uzelac, N. Otani, S. Luther, R. F. Gilmour, E. M. Cherry, F. H. Fenton, Synchronization as a mechanism for low-energy antifibrillation pacing, Heart Rhythm 14 (2017) 1254–62.

[16] A. H. Janardhan, W. Li, V. V. Fedorov, M. Yeung, M. J. Wallendorf, R. B. Schuessler, I. R. Efimov, A novel low-energy electrotherapy that terminates ventricular tachycardia with lower energy than a biphasic shock when antitachycardia pacing fails, Journal of the American College of Cardiology 60 (2012) 2393–8.

[17] S. Luther, F. H. Fenton, B. G. Kornreich, A. Squires, P. Bittihn, D. Hornung, M. Zabel, J. Flanders, A. Gladuli, L. Campoy, E. M. Cherry, G. Luther, G. Hasenfuss, V. I. Krinsky, A. Pumir, R. F. Gilmour, E. Bodenschatz, Low-energy control of electrical turbulence in the heart, Nature 475 (2011) 235–9.

[18] F. O. Campos, J. Whitaker, R. Neji, S. Roujol, M. O'Neill, G. Plank, M. J. Bishop, Factors Promoting Conduction Slowing as Substrates for Block and Reentry in Infarcted Hearts, Biophysical Journal 117 (2019) 2361–74.

[19] M. Jolley, J. Stinstra, J. Tate, S. Pieper, R. MacLeod, L. Chu, P. Wang, J. K. Triedman, Finite element modeling of subcutaneous implantable defibrillator electrodes in an adult torso, Heart Rhythm 7 (2010) 692–8.

[20] E. K. Heist, A. Belalcazar, W. Stahl, T. F. Brouwer, R. E. Knops, Determinants of Subcutaneous ImplantableÂăCardioverter-Defibrillator Efficacy: A Computer Modeling Study, JACC: Clinical Electrophysiology 3 (2017) 405–14.

[21] A. M. Plancke, A. Connolly, P. M. Gemmell, A. Neic, L. C. McSpadden, J. Whitaker, M. O'Neill, C. A. Rinaldi, R. Rajani, S. A. Niederer, G. Plank, M. J. Bishop, Generation of a cohort of whole-torso cardiac models for assessing the utility of a novel computed shock vector efficiency metric for ICD optimisation, Computers in Biology and Medicine 112 (2019) 103368.

[22] D. J. Swenson, R. T. Taepke, J. J. Blauer, E. Kwan, E. Ghafoori, G. Plank, E. Vigmond, R. S. MacLeod, P. DeGroot, R. Ranjan, Direct comparison of a novel antitachycardia pacing algorithm against present methods using virtual patient modeling, Heart Rhythm 17 (2020) 1602–8.

[23] A. Connolly, S. Williams, K. Rhode, C. A. Rinaldi, M. J. Bishop, Conceptual intra-cardiac electrode configurations that facilitate directional cardiac stimulation for optimal electrotherapy, IEEE Transactions on Biomedical Engineering 66 (2019) 1259–68.

[24] M. Jolley, J. Stinstra, S. Pieper, R. MacLeod, D. H. Brooks, F. Cecchin, J. K. Triedman, A computer modeling tool for comparing novel ICD electrode orientations in children and adults, Heart Rhythm 5 (2008) 565–72.

[25] V. Jayam, M. Zviman, V. Jayanti, A. Roguin, H. Halperin, R. D. Berger, Internal defibrillation with minimal skeletal muscle activation: A new paradigm toward painless defibrillation, Heart Rhythm 2 (2005) 1108–13.

[26] J. Whitaker, R. Neji, N. Byrne, E. Puyol-Antón, R. K. Mukherjee, S. E. Williams, H. Chubb, L. O'Neill, O. Razeghi, A. Connolly, K. Rhode, S. Niederer, A. King, C. Tschabrunn, E. Anter, R. Nezafat, M. J. Bishop, M. O'Neill, R. Razavi, S. Roujol, Improved co-registration of ex-vivo and in-vivo cardiovascular magnetic resonance images using heart-specific flexible 3D printed acrylic scaffold combined with non-rigid registration, Journal of Cardiovascular Magnetic Resonance 21 (2019) 1–15.

[27] A. Neic, M. A. F. Gsell, E. Karabelas, A. J. Prassl, G. Plank, Automating image-based mesh generation and manipulation tasks in cardiac modeling workflows using meshtool, SoftwareX 11 (2020) 100454.

[28] J. D. Bayer, R. C. Blake, G. Plank, N. A. Trayanova, A novel rule-based algorithm for assigning myocardial fiber orientation to computational heart models, Annals of Biomedical Engineering 40

(2012) 2243–54.

[29] E. J. Vigmond, M. Hughes, G. Plank, L. J. Leon, Computational Tools for Modeling Electrical Activity in Cardiac Tissue, Journal of Electrocardiology 36 (2003) 69–74.

[30] C. S. Henriquez, Simulating the electrical behavior of cardiac tissue using the bidomain model., Critical reviews in biomedical engineering 21 (1993) 1.

[31] L. Clerc, Directional differences of impulse spread in trabecular muscle from mammalian heart., The Journal of Physiology 255 (1976) 335–46.

[32] A. J. Connolly, M. J. Bishop, Computational Representations of Myocardial Infarct Scars and Implications for Arrhythmogenesis, Clinical Medicine Insights: Cardiology 10s1 (2016) 27–40.

[33] P. Colli-Franzone, V. Gionti, L. F. Pavarino, S. Scacchi, C. Storti, Role of infarct scar dimensions, border zone repolarization properties and anisotropy in the origin and maintenance of cardiac reentry, Mathematical Biosciences 315 (2019) 108228.

[34] K. H. Ten Tusscher, A. V. Panfilov, Alternans and spiral breakup in a human ventricular tissue model, American Journal of Physiology - Heart and Circulatory Physiology 291 (2006) 1088–100.

[35] R. Peinado, T. Rius, A. Moya, J. L. Merino, A. Arenal, L. Tercedor, O. Medina, Randomized , Prospective Comparison of Four Burst Ventricular Tachycardia 82 (1998) 1422–5.

[36] J. Jiménez-Candil, J. Hernández, A. Martín, M. Ruiz-Olgado, J. Herrero, C. Ledesma, J. Moríñigo, C. Martín-Luengo, Influence of beta-blocker therapy on antitachycardia pacing effectiveness for monomorphic ventricular tachycardias occurring in implantable cardioverter-defibrillator patients: A dose-dependent effect, Europace 12 (2010) 1231–8.

[37] V. Semmler, J. Biermann, B. Haller, C. Jilek, N. Sarafoff, C. Lennerz, H. Vrazic, B. Zrenner, S. Asbach, C. Kolb, ICD shock, not ventricular fibrillation, causes elevation of high sensitive troponin T after defibrillation threshold testing-the prospective, randomized, multicentre tropshock-trial, PLoS ONE 10 (2015) 1–15.

[38] D. Birnie, S. Tung, C. Simpson, E. Crystal, D. Exner, F. A. Ayala Paredes, A. Krahn, R. Parkash, Y. Khaykin, F. Philippon, P. Guerra, S. Kimber, D. Cameron, J. S. Healey, Complications associated with defibrillation threshold testing: The Canadian experience, Heart Rhythm 5 (2008) 387–90.

[39] J. T. Niemann, R. G. Walker, J. P. Rosborough, Intracardiac voltage gradients during transthoracic defibrillation: Implications for postshock myocardial injury, Academic Emergency Medicine 12 (2005) 99–105.

[40] D. Andreu, J. Fernández-Armenta, J. Acosta, D. Penela, B. Jáuregui, D. Soto-Iglesias, V. Syrovnev, E. Arbelo, J. M. Tolosana, A. Berruezo, A QRS axisâĂŞbased algorithm to identify the origin of scar-related ventricular tachycardia in the 17-segment American Heart Association model, Heart Rhythm 15 (2018) 1491–7.

[41] S. Monaci, K. Gillette, E. Puyol-Antón, R. Rajani, G. Plank, A. King, M. Bishop, Automated Localization of Focal Ventricular Tachycardia From Simulated Implanted Device Electrograms: A Combined PhysicsâĂŞAI Approach, Frontiers in Physiology 12 (2021) 1–15.

[42] J. K. Steffen, P. Reker, F. K. Mennicken, T. A. Dembek, H. S. Dafsari, G. R. Fink, V. Visser-Vandewalle, M. T. Barbe, Bipolar Directional Deep Brain Stimulation in Essential and Parkinsonian Tremor, Neuromodulation 23 (2020) 543–9.

[43] G. Deli, I. Balas, F. Nagy, E. Balazs, J. Janszky, S. Komoly, N. Kovacs, Comparison of the efficacy of unipolar and bipolar electrode configuration during subthalamic deep brain stimulation, Parkinsonism and Related Disorders 17 (2011) 50–4.

[44] A. Moreno, R. D. Walton, J. D. Bayer, Stretchable Conductive Fabric for Cardiac Electrophysiology Applications, ACS Applied Bio Materials 3 (2020) 3114–22.

[45] M. Han, L. Chen, K. Aras, C. Liang, X. Chen, H. Zhao, K. Li, N. R. Faye, B. Sun, J. H. Kim, W. Bai, Q. Yang, Y. Ma, W. Lu, E. Song, J. M. Baek, Y. Lee, C. Liu, J. B. Model, G. Yang, R. Ghaffari, Y. Huang, I. R. Efimov, J. A. Rogers, Catheter-integrated soft multilayer electronic arrays for multiplexed sensing and actuation during cardiac surgery, Nature Biomedical Engineering 4 (2020) 997–1009.

[46] P. Gutruf, R. T. Yin, K. B. Lee, J. Ausra, J. A. Brennan, Y. Qiao, Z. Xie, R. Peralta, O. Talarico, A. Murillo, S. W. Chen, J. P. Leshock, C. R. Haney, E. A. Waters, C. Zhang, H. Luan, Y. Huang, G. Trachiotis, I. R. Efimov, J. A. Rogers, Wireless, battery-free, fully implantable multimodal and multisite pacemakers for applications in small animal models, Nature Communications 10 (2019).

[47] H. Fang, K. J. Yu, C. Gloschat, Z. Yang, E. Song, C. H. Chiang, J. Zhao, S. M. Won, S. Xu, M. Trumpis, Y. Zhong, S. W. Han, Y. Xue, D. Xu, S. W. Choi, G. Cauwenberghs, M. Kay, Y. Huang, J. Viventi, I. R. Efimov, J. A. Rogers, Capacitively coupled arrays of multiplexed flexible silicon transistors for long-term cardiac electrophysiology, Nature Biomedical Engineering 1 (2017).

A. Appendix

Here shows the full results of individual strengths required by both bipolar and transmural configurations to terminate all 6 VTs as in Figure S1. As is shown, the strength required for terminating VTs varies significantly in different VTs. In Figure S1(a), it shows that for bipolar configuration, at the delivery time of 88% VTCL, the strength to achieve partially high efficacy S_{pEff} is 860 V, while the strength to achieve full efficacy S_{fEff} is 1700V. The strengths S_{pEff} and S_{fEff} for transmural configuration are 80 V and 120 V as shown in Figure S1(b).

(a)
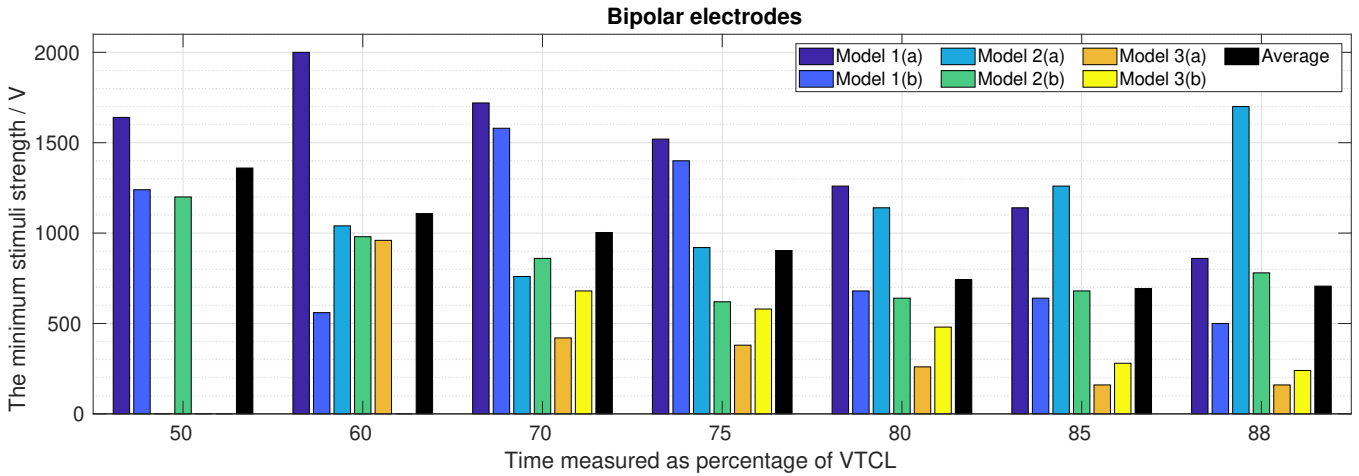
(b)
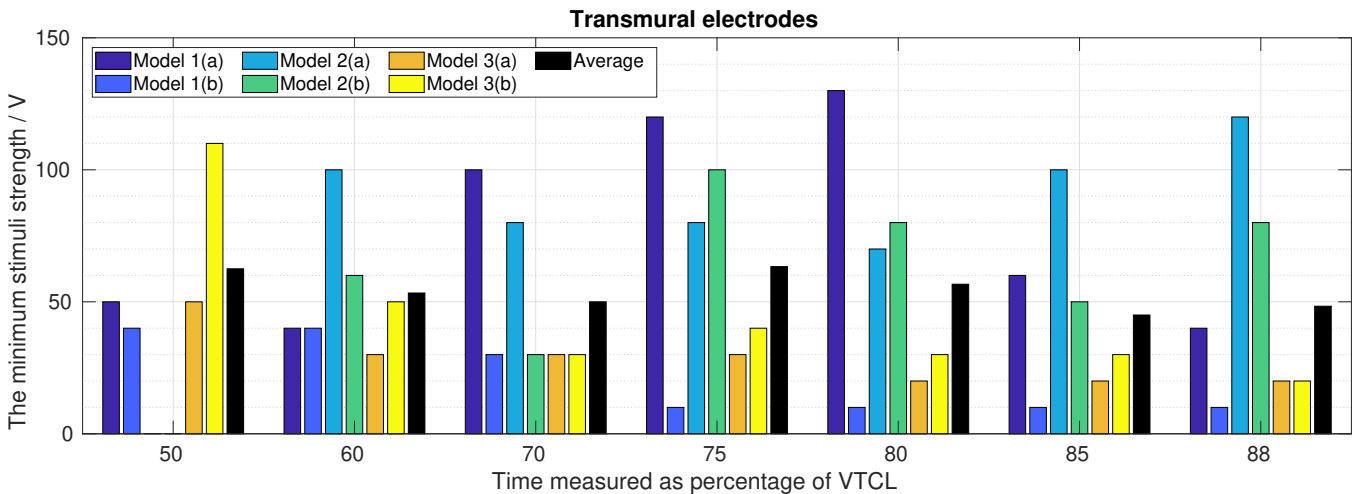
Figure S1: Minimum stimulus strength needed for terminating VT in (panel a) bipolar electrodes and (panel b) transmural electrodes were plotted against the pacing time defined as the percentage of the VTCL since the last activation detected at the CI. 6 VTs were tested and their average minimum stimulus strength at each pacing times were shown in black. Noted that at 50% and 60% of VTCL, some VTs were not terminated even the stimulus strength increasing until the computational simulation crashed. Therefore, the average value is calculated by eliminating those unsuccessful cases.